OPEN ACCESS
CellPress

Cell Reports
Report

A Dynamin Mutant Defines a Superconstricted Prefission State

Anna C. Sundborger,[1] Shunming Fang,[1] Jürgen A. Heymann,[1] Pampa Ray,[1] Joshua S. Chappie,[2,*] and Jenny E. Hinshaw[1,*]

[1]Laboratory of Cell and Molecular Biology, National Institute of Diabetes and Digestive and Kidney Diseases, National Institutes of Health, Bethesda, MD 20892, USA

[2]Department of Molecular Medicine, College of Veterinary Medicine, Cornell University, Ithaca, NY 14850, USA

*Correspondence: chappie@cornell.edu (J.S.C.), jennyh@helix.nih.gov (J.E.H.)

http://dx.doi.org/10.1016/j.celrep.2014.06.054

SUMMARY

Dynamin is a 100 kDa GTPase that organizes into helical assemblies at the base of nascent clathrin-coated vesicles. Formation of these oligomers stimulates the intrinsic GTPase activity of dynamin, which is necessary for efficient membrane fission during endocytosis. Recent evidence suggests that the transition state of dynamin's GTP hydrolysis reaction serves as a key determinant of productive fission. Here, we present the structure of a transition-state-defective dynamin mutant K44A trapped in a prefission state at 12.5 Å resolution. This structure constricts to 3.7 nm, reaching the theoretical limit required for spontaneous membrane fission. Computational docking indicates that the ground-state conformation of the dynamin polymer is sufficient to achieve this superconstricted prefission state and reveals how a two-start helical symmetry promotes the most efficient packing of dynamin tetramers around the membrane neck. These data suggest a model for the assembly and regulation of the minimal dynamin fission machine.

INTRODUCTION

Dynamin is a mechanochemical GTPase that assembles around the necks of invaginated clathrin-coated pits to catalyze membrane fission during the final stages of clathrin-mediated endocytosis (CME) (Ferguson and De Camilli, 2012; Schmid and Frolov, 2011; van der Bliek and Payne, 2010). Dynamin consists of a catalytic G domain connected to a membrane-binding pleckstrin homology (PH) domain through a helical stalk (middle domain and GTPase effector domain [GED]) (Figures 1A and 1B) (Faelber et al., 2011; Ford et al., 2011). At the C terminus, a proline- and arginine-rich domain (PRD) is present through which dynamin partners interact. In this arrangement, the GED's C terminus (C_{GED}) associates with the N and C termini of the G domain (N_{GTPase} and C_{GTPase}, respectively) to form the bundle signaling element (BSE) (Chappie et al., 2009) (Figures 1A and 1B, cyan). Structural analysis of a minimal G domain-GED fusion protein (GG) revealed that G domain dimerization optimally positions dynamin's catalytic machinery, leading to enhanced catalytic turnover (Chappie et al., 2010). In addition, the BSE undergoes a dramatic hydrolysis-dependent conformational change that may function as a dynamin powerstroke (Chappie et al., 2011). G domain dimerization is an intermolecular interaction and only occurs between tetramers in adjacent rungs of the helical assembly (Chappie et al., 2011; Faelber et al., 2011; Ford et al., 2011). Thus, the architecture of the dynamin polymer ensures that assembly and stimulated turnover are tightly coupled.

It remains unclear how the GTP hydrolysis cycle of dynamin translates to structural changes to promote membrane fission. Dynamin generates high membrane curvature and imposes localized strain on the inner monolayer of the membrane when assembled (Bashkirov et al., 2008; Roux et al., 2010; Schmid and Frolov, 2011). This asymmetric distribution of membrane stress has been predicted to promote a hemifission intermediate if the inner luminal diameter of the neck approaches the bilayer thickness (~4 nm) (Kozlovsky and Kozlov, 2003). Therefore, in the absence of physical constraints, an inner lumen of 4 nm could lead to spontaneous membrane fission (Bashkirov et al., 2008; Kozlovsky and Kozlov, 2003). Previous studies have visualized intermediates along the fission pathway. Wild-type dynamin (^{WT}Dyn) in the absence of nucleotide and truncated dynamin in the presence of β-γ-methyleneguanosine 5′-triphosphate (GMPPCP) ($^{\Delta PRD}Dyn_{GMPPCP}$) form protein-lipid tubes with inner luminal diameters of 20 nm and 7 nm, respectively (Chappie et al., 2011; Sweitzer and Hinshaw, 1998). The structure of the final prefission state where the inner lumen reaches 4 nm and the conformational changes necessary to achieve it remain a mystery.

Recent findings suggest that structural rearrangements in the dynamin polymer associated with the transition state may serve as a key determinant of productive fission (Schmid and Frolov, 2011; Chappie and Dyda, 2013). To examine these structural changes and understand how they contribute to membrane fission, we solved the structure of a transition-state-defective human dynamin 1 mutant (^{K44A}Dyn). This structure displays a two-start helical symmetry and is tightly constricted with an inner luminal diameter of 3.7 nm, reaching the theoretical limit for spontaneous fission. Computational docking reveals that a ground-state conformation of the hydrolysis reaction is sufficient to achieve this final "superconstricted" state and shows how the

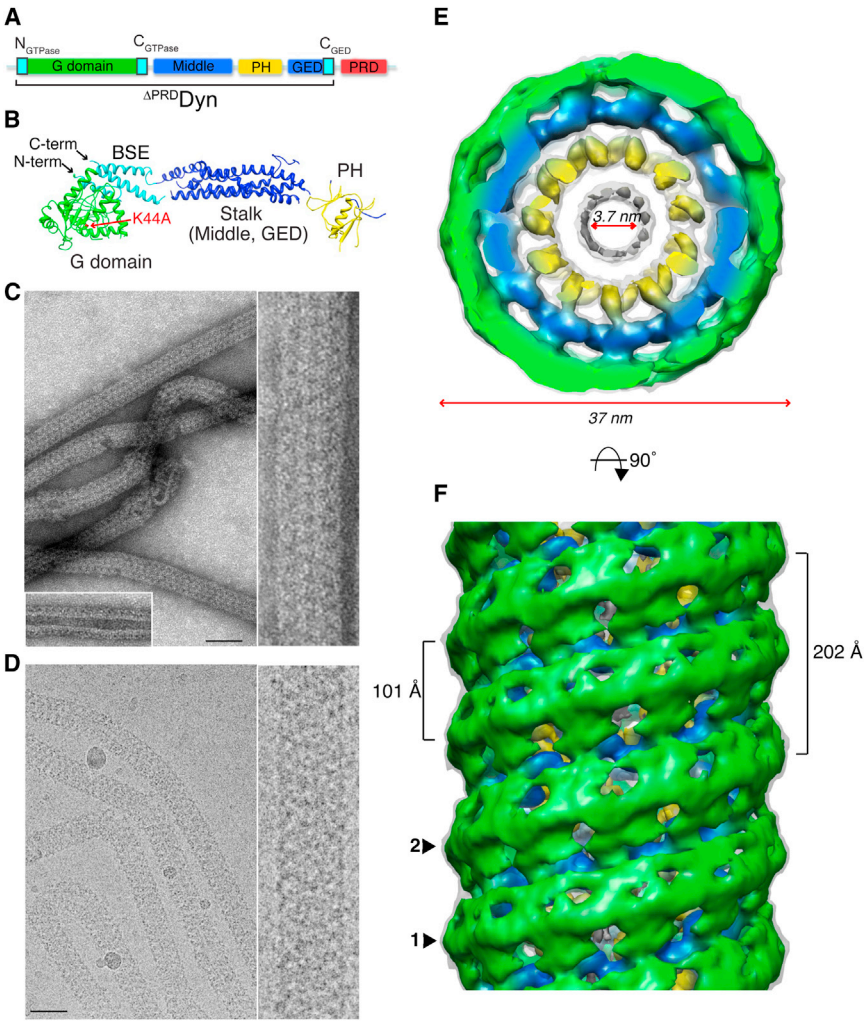

Figure 1. 3D Reconstruction of Superconstricted $^{K44A}Dyn_{GTP}$ Lipid Tubes

(A) Domain structure of dynamin, illustrating the conserved domains: G domain (green), middle domain (blue), pleckstrin homology domain (PH, yellow), GTPase effector domain (GED, blue), and the proline- and arginine-rich domain (PRD, red). The G domain N and C termini (N_{GTPase}, C_{GTPase}) and GED C terminus (C_{GED}) assemble into the bundle-signaling element (BSE) (cyan).

(B) Crystal structure of nucleotide-free human dynamin 1 (Faelber et al., 2011) (PDB ID 3SNH) showing the organization of the protein with an alternative PH domain assignment (Chappie and Dyda, 2013). The position of the K44A single mutation in the G domain (red arrow), the assembled BSE (cyan), and the N and C termini are labeled.

(C and D) Negative-stain (C) and cryo-EM (D) images of well-ordered $^{K44A}Dyn_{GTP}$ tubes at low (left) and high (right) magnifications. Inset in (C) shows ^{K44A}Dyn tubes in the absence of GTP. Scale bars, 50 nm.

(E) End view of the $^{K44A}Dyn_{GTP}$ 3D density map. The map is subdivided into three radial densities colored green, blue, and yellow. The outer diameter is 37 nm, while the inner lumen is 3.7 nm.

(F) Side view of the $^{K44A}Dyn_{GTP}$ 3D map shows how $^{K44A}Dyn_{GTP}$ assembles as a two-start helix labeled 1 and 2 with a helical pitch of 202 Å and an axial distance between neighboring subunits of 101 Å.

two-start helical arrangement generates the most efficient packing of dynamin tetramers around the membrane neck. Together, these data support a model for dynamin-catalyzed membrane fission that requires a transition-state-dependent conformational change to proceed successfully.

RESULTS

K44A Dynamin Tubes Constrict to 3.7 nm in the Presence of GTP

^{K44A}Dyn elicits a strong dominant-negative effect in vivo that blocks CME and impairs the assembly-stimulated GTPase activity of dynamin in vitro (Damke et al., 1994). ^{K44A}Dyn retains the ability to tubulate liposomes (Figure 1C and 1D), making it an ideal candidate for examining nucleotide-dependent conformations of the assembled polymer. Like ^{WT}Dyn, ^{K44A}Dyn generates protein-lipid tubes with an inner luminal diameter of ~20 nm in the absence of nucleotide (Figure 1C, inset). Addition of GTP to ^{K44A}Dyn tubes ($^{K44A}Dyn_{GTP}$) induces a constriction far beyond what has previously been reported for other dynamin variants (Figure 1C and 1D). Sedimentation assays indicate that ^{K44A}Dyn superconstricted tubes are stable in the presence of GTP, whereas ^{WT}Dyn disassociates from the lipid rapidly (Figure S1A) (Warnock et al., 1996). ^{WT}Dyn also forms superconstricted tubes in the presence of GTP, though they are short-lived and less stable (Figures S1B). Tilt series of dynamin tubes ($^{K44A}Dyn_{GTP}$, $^{\Delta PRD}$Dyn, $^{\Delta PRD}Dyn_{GMPPCP}$, $^{WT}Dyn_{GTP}$) revealed them all to be right-handed (Figure S1C; Chappie et al., 2011; Chen et al., 2004; Zhang and Hinshaw, 2001), suggesting this property is inherent to the assembled dynamin oligomer and does not change as a consequence of superconstriction.

The prolonged stability of $^{K44A}Dyn_{GTP}$ tubes allowed us to solve its structure by cryo-electron microscopy (cryo-EM) (Figure 1D). The 3D map was calculated using the iterative helical real-space method (IHRSR) (Egelman, 2007) to yield a 12.5 Å reconstruction (Figures 1E and 1F) with 11.8 subunits per turn (Table S1). The map was generated from tube segments with outer diameters of 35–36 nm and with an even projection distribution (Figures S1D and S1E). As with previous reconstructions (Chappie et al., 2011; Chen et al., 2004; Zhang and Hinshaw, 2001), the $^{K44A}Dyn_{GTP}$ polymer contains three radial densities (Figures 1E and 2): an inner density embedded in the outer leaflet of the lipid bilayer (yellow), a middle density that stabilizes the helical packing (blue), and an outer density that provides connectivity between the rungs of the helix (green). However, this map presents two unique features. First, ^{K44A}Dyn assembles

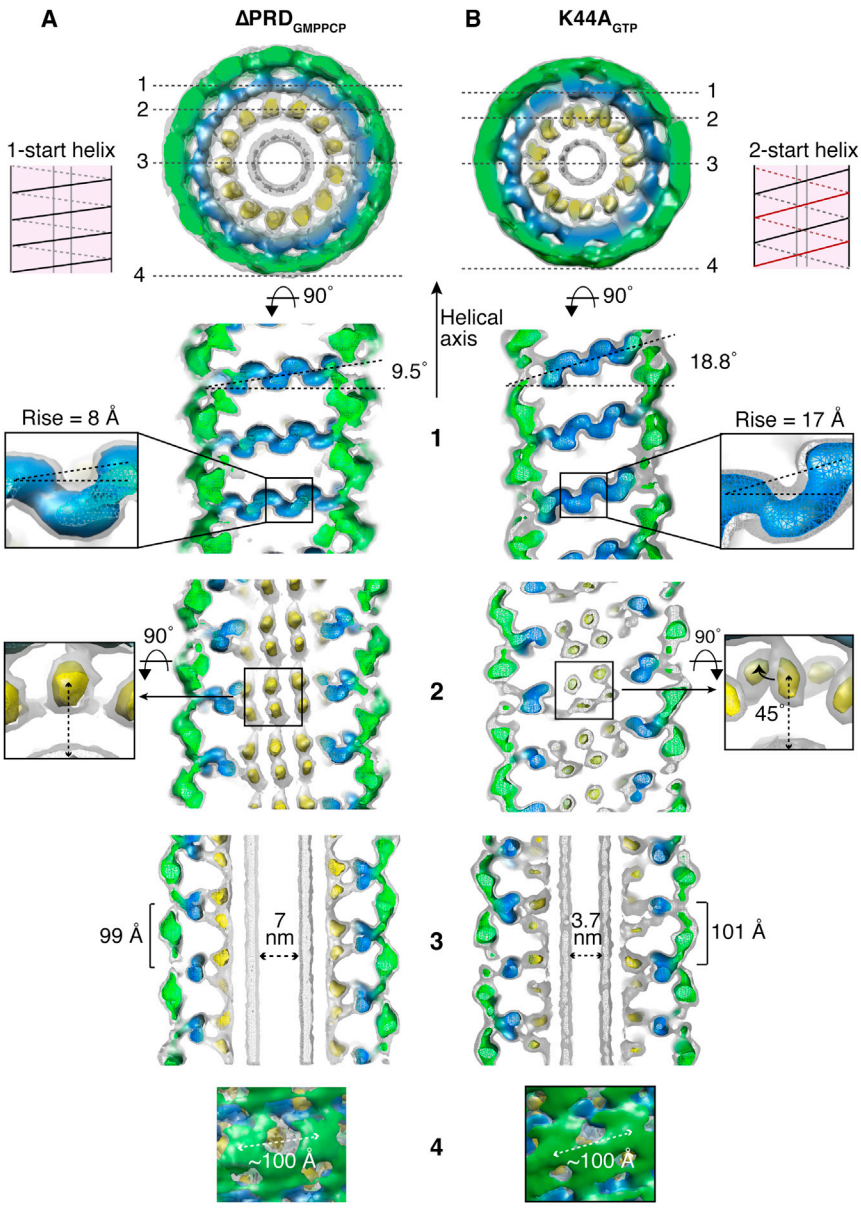

Figure 2. Structural Changes that Promote Superconstriction

Sections (1–4) through the $^{\Delta PRD}Dyn_{GMPPCP}$ (A) and $^{K44A}Dyn_{GTP}$ (B) 3D maps, as marked in the end view, are shown in greater detail below. Schematic diagrams (pink) illustrate the respective one-start (ΔPRD_{GMPPCP}) and two-start ($K44A_{GTP}$) helical symmetries. (1) The rise per subunit of the helix differs from 8 Å (A) to 17 Å (B) (insets). The angle perpendicular to the tube axis increases from 9.5° (A) to 18.8° (B). (2) In the inner radial region of $^{K44A}Dyn_{GTP}$, one density of the PH domain pair is tilted 45° out of the membrane (insets). (3) The inner luminal diameter is significantly smaller in the $^{K44A}Dyn_{GTP}$ tubes (3.7 nm) compared to $^{\Delta PRD}Dyn_{GMPPCP}$ tubes (7 nm). The axial distance between neighboring subunits is slightly larger in $^{K44A}Dyn_{GTP}$ tubes (101 Å compared to 99 Å). (4) The lateral packing (~100 Å) between the subunits remains constant.

into a two-start helix in the presence of GTP, whereas all previous reconstructions display a one-start helical symmetry (Figure 1F, labeled 1 and 2). The difference between the one-start and two-start helix is evident from the Fourier transforms of the helical tubes (Figure S2A, dotted lines). The two-start helix effectively doubles the helical pitch to 202 Å (Figures 1F; Table S1) without altering the lateral packing distance between subunits along the helical path (~100 Å) (Figure 2, section 4; Table S1) or the distance between neighboring rungs (~100 Å) (Figure 2, section 3; Table S1). Second, the ^{K44A}Dyn polymer has an outer diameter of 37 nm and an inner luminal diameter of 3.7 nm (Figure 1E; Table S1). $^{WT}Dyn_{GTP}$ tubes also display a two-start helical symmetry and constrict to ~4–6 nm, albeit transiently (Figure S2B).

Structural Changes that Promote Superconstriction

To identify architectural changes leading to superconstriction, we compared our $^{K44A}Dyn_{GTP}$ 3D map to "constricted" $^{\Delta PRD}$Dyn tubes stabilized by GMPPCP (Chappie et al., 2011). $^{\Delta PRD}Dyn_{GMPPCP}$ tubes form a one-start helix with an inner luminal diameter of 7 nm and an outer diameter of 40 nm, with 13.2 subunits per turn and a pitch of 99 Å (Table S1). Juxtaposition of $^{K44A}Dyn_{GTP}$ and $^{\Delta PRD}Dyn_{GMPPCP}$ shows that formation of a two-start helix in $^{K44A}Dyn_{GTP}$ is driven by an increase in the subunit rise from ~8 Å to ~17 Å (Figure 2, section 1, insets; Table S1). This reduces the number of subunits per turn without significantly altering the distance between subunits (Table S1). Instead, the entire stalk density of $^{K44A}Dyn_{GTP}$ within each rung tilts ~19° relative to the helical axis (Figure 2B, section 1, blue; Figure S2C, Leg), which causes a displacement of the inner leg densities in the same direction (Figure 2B, section 2, yellow). In addition, one leg density within a pair rotates 45° out of the plane of the membrane (Figure 2B, section 2, inset).

$^{K44A}Dyn_{GTP}$ Superconstricted Tubes Are Trapped in a Ground-State Conformation

To describe the molecular changes that occur within individual dynamin subunits of the superconstricted $^{K44A}Dyn_{GTP}$ map, we performed computational docking using the YUP software package (Tan et al., 2008) to generate a pseudoatomic model of the $^{K44A}Dyn_{GTP}$ polymer (Figure 3). The cryo-EM density could not accommodate the available intact dynamin crystal structures (Faelber et al., 2011; Ford et al., 2011) (data not shown), and thus individual dynamin domain structures were positioned

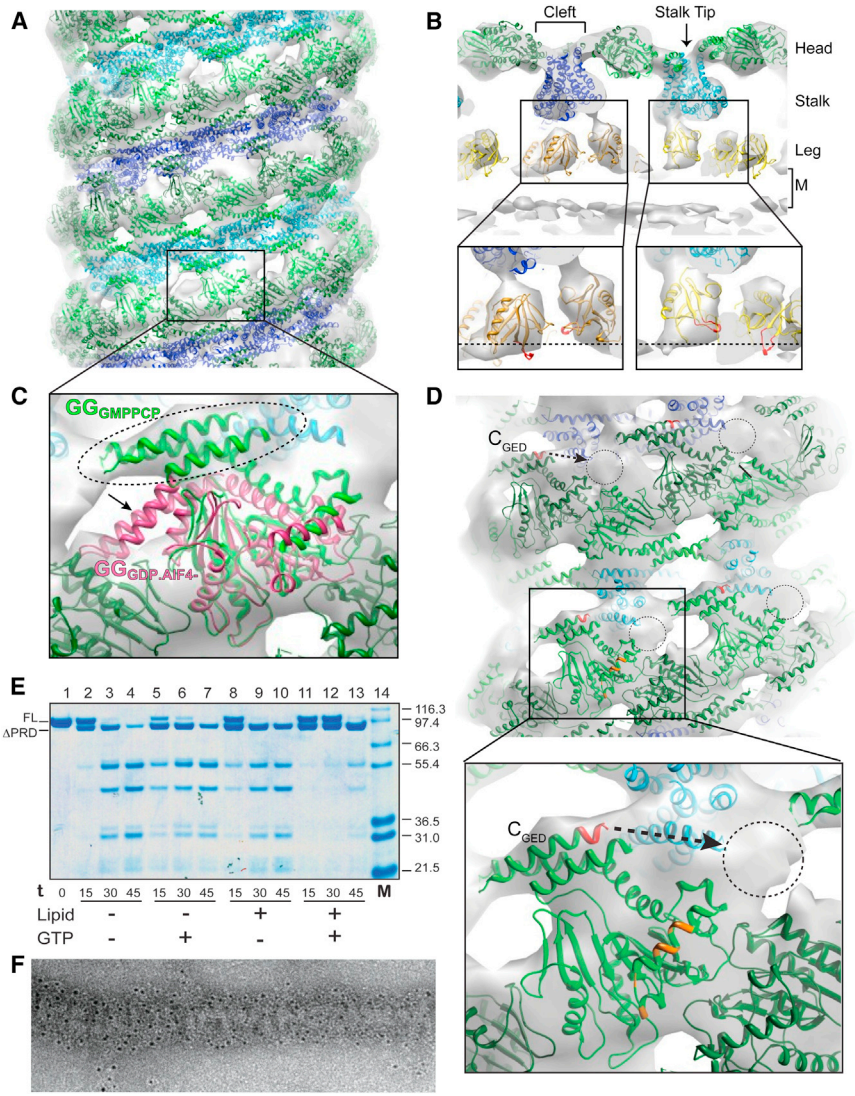

Figure 3. Pseudoatomic Model of the $^{K44A}Dyn_{GTP}$ Polymer

(A) Side view of $^{K44A}Dyn_{GTP}$ 3D map showing docked GG dimers (PDB ID 3ZYC, green), stalks (truncated from PDB ID 3SNH, blue and cyan), and the PH domains (PDB ID 1DYN, yellow).

(B) Cross-section "T-view" of the 3D map with the three radial densities (Head, Stalk, and Leg) marked and the membrane labeled "M." The cleft between the G domains and the stalk tip are also noted. PH domains are positioned with variable loop 1 (colored red) either inserted into the outer leaflet or tilted away from the membrane by 45° (insets). Dashed lines shows presumed position of the outer boundary of the lipid bilayer (insets).

(C) The GG_{GMPPCP} (PDB ID 3ZYC; green) crystal structure fits well into the 3D map with the BSE in the upward configuration (dashed oval) while the $GG_{GDP/AlF-}$ BSE (magenta; PDB ID 2X2E) extends out of the density (dashed arrow).

(D) Side views of the $^{K44A}Dyn_{GTP}$ docking reveals an empty density (dashed circles) that may be occupied by the PRD. The relative position of GED's C terminus (red) and proximity (dashed arrow) is shown in the inset. The putative PRD site (dashed circle) is also close to a conserved, surface-accessible region in the G domain (inset, orange).

(E) Limited proteolysis of ^{K44A}Dyn (FL indicates full length) by trypsin over time (0–45 min) in the absence (lanes 2–7) and presence (lanes 8–13) of lipid, and with (lanes 5–7; 11–13) or without GTP (lanes 2–4; 8–10). The assembled state of $^{K44A}Dyn_{GTP}$ protects the protein from trypsin digest with the exception of the PRD (ΔPRD; lanes 11–13).

(F) Immunogold labeling of $^{K44A}Dyn_{GTP}$ lipid tubes using a PRD-specific antibody specifically labeled the outer surface of $^{K44A}Dyn_{GTP}$ lipid tubes.

using a combination of manual and flexible fitting procedures (Mears et al., 2007; Tan et al., 2008). As with previous reports (Chappie et al., 2011; Faelber et al., 2011; Ford et al., 2011; Mears et al., 2007), the G domain and BSE fit into the outer head density (green), the middle domain and GED fit into the stalk density (blue), and the PH domain occupies the leg density (yellow) (Figures 3A and 3B). Half of the PH domains are tilted such that variable loop 1 (Figure 3C, inset, colored red), which normally penetrates the outer leaflet of the bilayer (Burger et al., 2000; Ramachandran and Schmid, 2008), is partially pulled out, weakening dynamin's association with the membrane (Figure 3B, insets, where dashed lines estimate the lipid bilayer boundary). The PH domains disrupt the outer leaflet of the bilayer, leading to a less defined density for the outer leaflet.

Multiple crystallographic models are available for dynamin in different nucleotide-bound states (Chappie et al., 2010, 2011; Faelber et al., 2011; Ford et al., 2011). These differ in the position of the BSE relative to the G domain core, with the helix bundle up in the nucleotide-loaded, prehydrolysis ground state and down in both the transition- and nucleotide-free states, assumed to represent a posthydrolysis state (Chappie and Dyda, 2013). Only the GMPPCP-bound conformation of the GG structure fits into our $^{K44A}Dyn_{GTP}$ map (Figure 3C, green). The BSE of $GG_{GPD.AlF4-}$ protrudes from the density (Figure 3C, magenta), suggesting that the individual subunits within superconstricted $^{K44A}Dyn_{GTP}$ tubes adopt a ground-state-like conformation. This is consistent with the K44 side chain being one of three critical catalytic components responsible for stabilizing dynamin's transition state (Chappie et al., 2011) (Figures S3A and S3B) and with our findings that mutating it in GG abolishes dimerization and catalytic activity (Figures S3C and S3D).

Putative Location of the PRD in the $^{K44A}Dyn_{GTP}$ 3D Map

Docking revealed a strong unoccupied density on the outer surface of the $^{K44A}Dyn_{GTP}$ tubes that cannot be accounted for with any of the existing dynamin crystal structures (Figures 3D). By

way of exclusion and considering its proximity to the C_{GED} (Figure 3D, dashed arrow), we interpret this density to be a portion of the flexible PRD. The following results support such placement of the PRD: (1) limited proteolysis indicates the PRD is exposed and cleavable in superconstricted $^{K44A}Dyn_{GTP}$ tubes (Figure 3E, compare lanes 8–10 to 11–13), and (2) an antibody against the PRD specifically labels the outer surface of constricted tubes (3 ± 0.08 gold particles/μm^2 tube versus 0.66 ± 0.048 gold particles/μm^2 background, average ± SEM, $n = 97$, $p < 0.001$) (Figure 3F). Little proteolysis is observed during the 30 min incubation with GTP, confirming that ^{K44A}Dyn is protected in the superconstricted state and does not disassociate and rebind to the lipid (Figure 3E, compare lanes 6 and 12). The putative position of the PRD is close to a conserved surface-accessible region of the G domain (Figure 3D, inset, orange) found only in dynamin and not in other dynamin-related proteins that lack a PRD.

The location and accessibility of the PRD may allow partners to modulate function even in the final stages of CME. To examine this, we superimposed the endophilin cryo-EM map (EMD-5367; Mim et al., 2012) with our K44A superconstricted map and measured the distance between the presumed positions of the PRD and the endophilin SH3 domain (Figure S4A). These segments are separated by ~8 nm. Biochemical mapping indicates that there are ~28 amino acids (residues 750 and 778 in human dynamin 1) between the end of the GED and the endophilin's binding motif in the PRD (Anggono and Robinson, 2007). This region is predicted to be unstructured (Figure S4B) and as such could span over 10.4 nm. Thus, it is conceivable that the two regions could physically interact within the constraints of the superconstricted state.

A Two-Start Helical Symmetry Generates a Preferred Packing of Dynamin Tetramers

To determine how the two-start symmetry of the superconstricted state impacts G domain dimerization, we colored the individual docked structures in the $^{K44A}Dyn_{GTP}$ map according to the presumed boundaries of the underlying tetramers (the building block of dynamin) and examined their arrangement within a single helical turn (Figure 4). While only six tetramers are required for one turn of the $^{K44A}Dyn_{GTP}$ helix, the increased pitch prevents G domain dimerization from occurring within a single strand (Figure 4A) as occurs in the one-start $^{\Delta PRD}Dyn_{GMPPCP}$ polymer (Figure 4C). Instead, the two-start symmetry dictates that the G domain dimers form between the two helical strands of the $^{K44A}Dyn_{GTP}$ assembly and generate a total of 19 such parings that are distributed equally around the neck (Figures 4B and 4D). A single turn of the one-start $^{\Delta PRD}Dyn_{GMPPCP}$ helix forms only four G domain dimers that are asymmetrically localized on one side of the tube (Figures 4C and 4E). Each dimer buries a surface area of 2,561Å^2 (Chappie et al., 2010), representing a significant free energy gain and additional physical association that could stabilize the assembly further in the longitudinal direction.

Structural superposition shows only minor differences between the docked ^{K44A}Dyn (green) and $^{\Delta PRD}$Dyn (blue) tetramers (Figure S4C), indicating that the overall domain organization and intramolecular interactions are preserved. The changes in packing instead appear to arise from different intermolecular interactions between tetramers, which cause them to slide and twist as rigid bodies to accommodate the helical expansion and radial compression associated with the superconstricted state (Figure S4D, dashed circles).

DISCUSSION

Dynamin family GTPases mediate numerous membrane fission and fusion events in the cell (Heymann and Hinshaw, 2009). In vitro studies have shown that dynamin alone can cause membrane fission in the presence of GTP (Bashkirov et al., 2008; Morlot et al., 2012; Pucadyil and Schmid, 2008) and have suggested that a transition state of dynamin's GTP hydrolysis reaction may be the key determinant of fission (Shnyrova et al., 2013). Here, we have structurally characterized a transition-state-defective dynamin mutant (^{K44A}Dyn) that consequently becomes trapped in a prefission complex. $^{K44A}Dyn_{GTP}$ helical tubes adopt a superconstricted conformation with an inner luminal diameter of only 3.7 nm. Similar results were observed with $^{WT}Dyn_{GTP}$, albeit transiently. Superconstriction is achieved by dynamin adopting a two-start helical organization, which has not been previously observed in reconstructions of dynamin polymers.

A two-start helical assembly offers several advantages for efficient membrane fission. First, the rise between subunits in the two-start helix is doubled, allowing for constriction to 3.7 nm without major changes in the basic building block of the polymer. Second, the two-start symmetry allows G domain dimers to form between the adjacent helical strands concomitant with polymer assembly. This maximizes the number of G domain dimers that can be formed within a single helical turn and ensures even distribution of these dimers around the membrane neck, effectively priming the system for coordinated stimulated GTP hydrolysis. The dynamin-related protein DNM1, which catalyzes mitochondrial fission in yeast, also adopts a two-start helical arrangement on membranes (Mears et al., 2011). How conserved this architecture is among other dynamin family members remains to be seen.

Computational docking shows that dynamin tetramers in the superconstricted state are stabilized in a ground-state conformation. This implies that constriction to the fission limit occurs without input from stimulated GTP hydrolysis and that subsequent fission requires progression through the transition state. Docking also identified an empty density on the surface of the $^{K44A}Dyn_{GTP}$ polymer that we predict represents the PRD. Localization of the PRD in this region allows for dynamin partners to bind throughout the entire endocytic process. These partners may facilitate dynamin assembly and the efficiency of a minimal fission complex. For example, endophilin has been shown to regulate dynamin assembly during synaptic vesicle recycling and may prime dynamin to assemble into a two-start helix at the necks of coated pits by increasing the pitch of the dynamin helix from 10 to 20 nm (Sundborger et al., 2011).

Our pseudoatomic model also shows that one of the PH domains in the asymmetric unit of the $^{K44A}Dyn_{GTP}$ map is tilted 45° perpendicular to the membrane axis, consistent with the concept that the PH domain undergoes a conformational change during fission. PH domain insertion into the plasma membrane is crucial for endocytosis, as mutants lacking this ability are dominant negative (Ramachandran et al., 2009). The PH domain can

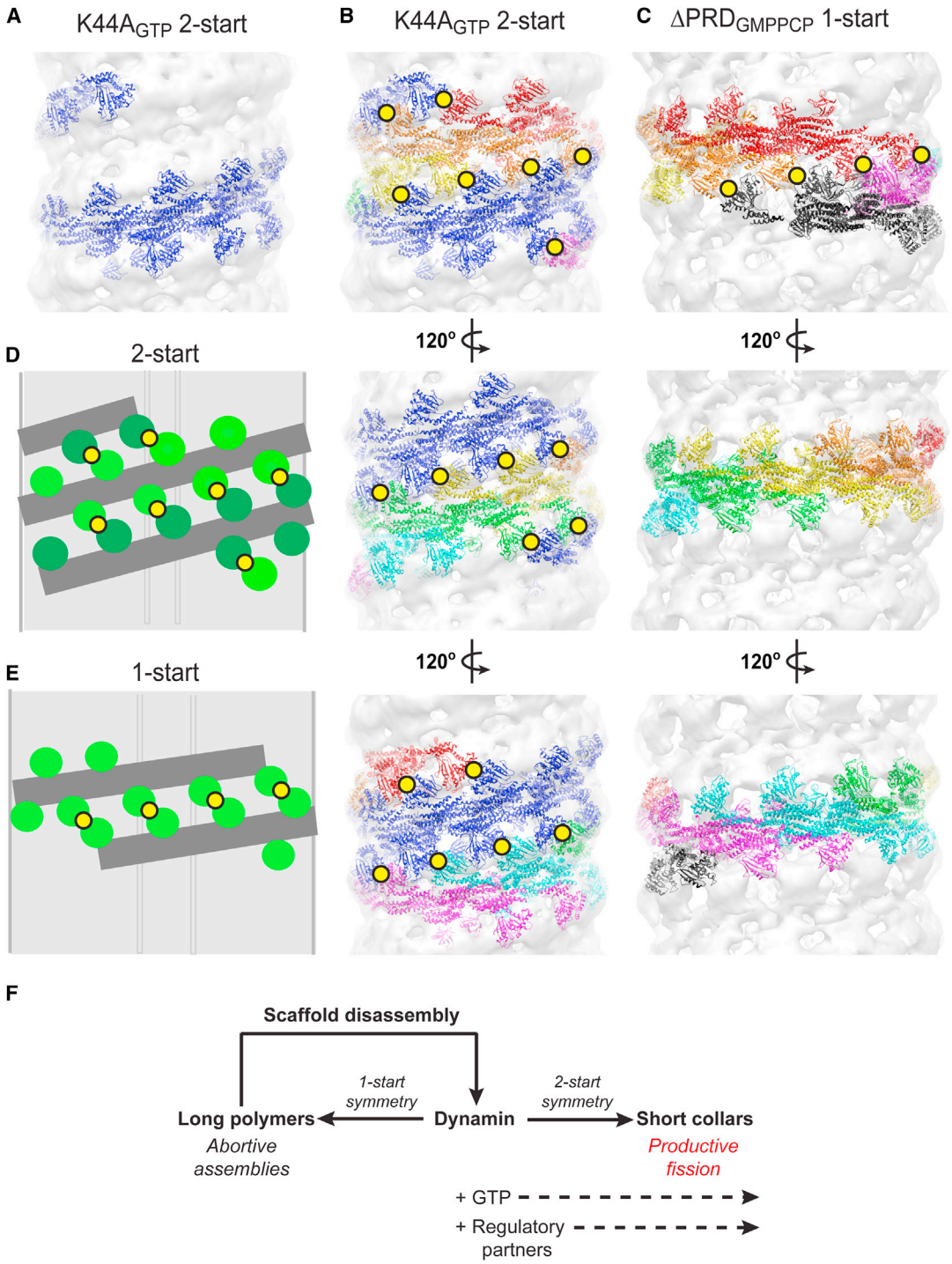

Figure 4. A Two-Start Helical Symmetry Generates Efficient Packing of Dynamin Tetramers

(A) Illustration of a single strand of the $^{K44A}Dyn_{GTP}$ two-start helix showing that G domain dimerization does not occur in a single strand wrapping around the membrane.

(B and C) Side-by-side comparison of a single turn of the $^{K44A}Dyn_{GTP}$ two-start polymer (B) and a single turn of the $^{\Delta PRD}Dyn_{GMPPCP}$ one-start polymer (C). Three rotations of each helix are shown (120 degrees each). In the $^{K44A}Dyn_{GTP}$ polymer, one strand is colored blue and the other is colored rainbow. Yellow circles denote G domain dimers formed in each assembly.

(D and E) Cartoon illustration of the subunits organization in a two- (D) and one-start (E) helix.

(F) Assembly of short dynamin collars with a two-start helical symmetry facilitates membrane fission. Long dynamin polymers assembled in the absence of GTP are abortive and unable to efficiently mediate fission.

also actively destabilize the lipid bilayer, possibly promoting the fission reaction (Bethoney et al., 2009; Ramachandran and Schmid, 2008; Shnyrova et al., 2013). We suggest that the PH domain rearrangement we observe in the superconstricted state represents either the initiation of the PH domain "tilting" proposed to evoke fission (Shnyrova et al., 2013) or the observed "retracted" state of the PH domain proposed to keep dynamin on the membrane surface during the GTP hydrolysis cycle (Mehrotra et al., 2014).

Recent studies estimate that the minimal fission machine consists of two turns of a one-start dynamin helix (Liu et al., 2013; Shnyrova et al., 2013). Based on our findings, we interpret the optimal minimal machinery to be a single turn of a two-start dynamin helix. We anticipate that the constant presence of GTP in the cell will bias dynamin toward the formation of short two-start helices (Figure 4F). Supporting this, we show that in vitro both $^{WT}Dyn_{GTP}$ and $^{K44A}Dyn_{GTP}$ assemble only into two-start helices. The one-start and two-start helical symmetries are discrete structural states and likely do not interconvert without complete disassembly of one scaffold and reassembly with the alternative symmetry. Therefore, the long one-start helices observed in vitro (Chappie et al., 2011, Chen et al., 2004, Zhang and Hinshaw, 2001) might not represent "true" fission intermediates. This distinction provides an explanation for in vitro observations that long dynamin assemblies inhibit fission and must undergo cycles of GTP hydrolysis to reach a critical minimal length to be productive (Bashkirov et al., 2008; Pucadyil and Schmid, 2008). These changes could be interpreted to represent a symmetry switch to the more efficient two-start packing (Figure 4F).

The $^{K44A}Dyn_{GTP}$ structure presented here provides insights into the mechanisms of dynamin-catalyzed membrane fission during CME. In the cell, assembly of dynamin in the presence of GTP promotes the formation of a two-start helix at the necks of coated pits that can reach the 4 nm fission barrier. The two-start helical symmetry also provides the optimal minimal configuration for G domain dimerization. G domain dimerization induces stimulated GTP hydrolysis and progression through the transition state, which serves as the key determinant of productive fission and leads to conformational changes that promote the physical scission event.

Though our findings shed light on the final prefission state of the dynamin polymer, the precise transition-state-dependent conformational changes within this assembly that trigger fission still remain to be elucidated. Previous structural studies revealed a dynamin powerstroke consisting of a hydrolysis-dependent BSE conformational change (Chappie et al., 2011). How the powerstroke propagates through the rest of the dynamin polymer and whether it is sufficient for the GTP-induced supercoiling and fragmentation observed in vitro remain to be determined (Danino et al., 2004; Roux et al., 2006). Moreover, biochemical studies suggest fission may be triggered by more subtle GTP-induced membrane remodeling events such as scaffold loosening and/or disassembly (Bashkirov et al., 2008; Pucadyil and Schmid, 2008), curvature-dependent changes in membrane elastic energy at the edge of the dynamin polymer (Morlot et al., 2012), or PH domain tilting within short metastable dynamin scaffolds (Shnyrova et al., 2013). These mechanisms are likely not mutually exclusive, and dynamin may use a combination of both mechanical force and membrane remodeling to drive fission. Future structural and biophysical studies will assist in unraveling the global conformational changes that are needed to move beyond the final superconstricted prefission state.

EXPERIMENTAL PROCEDURES

Cryo-Electron Microscopy Imaging

A 3.5 μl sample of $^{K44A}Dyn_{GTP}$ lipid tubes was placed on a plasma-cleaned (Fishione) Quantifoil holey carbon electron microscopy grid (SPI Supplies), blotted with filter paper, and flash-frozen in liquid ethane using a Leica EM GP (Leica Microsystems). The vitrified samples were imaged at liquid nitrogen temperature on a Polara FEG electron microscope (FEI Company) operating at 200 kV and recorded at 49,000× magnification. Images were recorded on Kodak SO163 film under low-dose conditions with defocus values ranging from −0.5 to 2 μm. Images were digitized using a NIKON supercool 9000 scanner at 80 ppm and 2.55 Å/pixel.

3D Reconstruction of $^{K44A}Dyn_{GTP}$ Lipid Tubes

Images were individually contrast transfer function corrected using the bsoft image-processing package (bshow and bctf, Cs = 2.26) (Heymann and Belnap, 2007). Well-ordered and straight $^{K44A}Dyn_{GTP}$ tubes were manually selected and processed with iterative helical real space reconstruction (IHRSR) methodology (Egelman, 2007) (see the Supplemental Experimental Procedures). The final map merged to a rotation angle of 30.59° and rise of 17.19 Å. The resolution of the final map was determined to be 12.5 Å by Fourier shell correlation (FSC = 0.5) and was calculated, using the new "gold standard" (Henderson, 2013), from 3D maps generated from half of the data randomized with two different reference models (a cylinder and a modified $^{\Delta PRD}$Dyn map) and two different starting parameters (rise and rotation).

Computational Docking

All-atom structures were refined using the YUP.SCX method of the YUP software package (Tan et al., 2008). Initial fitting was performed using GG_{GMPPCP} monomers (Protein Data Bank [PDB] ID 3ZYC; Chappie et al., 2011), dynamin middle/GED stalk monomers (PDB ID 3SNH; Faelber et al., 2011), and PH domain monomers (PDB ID 1DYN; Ferguson et al., 1994). Orientations of the middle/GED and PH monomers were largely unchanged compared to previous docked maps (Chappie et al., 2011; Faelber et al., 2011; Ford et al., 2011) and the GG_{GMPPCP} placement refined to a single orientation that best matched the $^{K44A}Dyn_{GTP}$ cryo-EM structure.

Limited Proteolysis

^{K44A}Dyn in HCB100 at 0.25 mg/ml was incubated with 1:500 w/w trypsin (Sigma Aldrich) at room temperature in the presence and absence of synthetic DOPS extruded liposomes and in the presence and absence of 1 mM GTP. Small aliquots were taken at intervals of 15 min after addition of trypsin to examine the amount of proteolysis that occurred over the course of 45 min. Samples were run on an SDS-PAGE and visualized using colloidal blue (Invitrogen).

Immunogold Labeling

Immunogold labeling of $^{K44A}Dyn_{GTP}$ lipid tubes was performed as previously described (Mears et al., 2007). In brief, ^{K44A}Dyn tubes were prepared as described above and incubated with 1 mM GTP for 30 min. The sample was applied to carbon-coated 400 mesh Cu/Rh grids for 1 min and subsequently blocked with HCB100 containing 1% BSA for 45 min. The grids were then incubated on a drop of Hudy-1 antibody (Upstate Biotech) for 1 hr and washed six times for 5 min each with HCB100. The grids were incubated with 6 nm colloidal gold rabbit anti-mouse secondary antibody for 1 hr followed by six 5 min washes with HCB100. The grids were stained with 1% uranyl acetate for 30 s. Images were taken on a CM120 transmission electron microscope (FEI Company) using low-dose conditions at 100 kV with a LaB_6 filament. Images were recorded using a Gatan 1k × 1k CCD camera. Labeling density was quantified as number of gold particles in a 500 μm^2 area (gold particles/μm^2)

and compared between dynamin lipid tubes, background, and samples labeled with secondary antibody alone.

SUPPLEMENTAL INFORMATION

Supplemental Information includes Supplemental Experimental Procedures, four figures, and one table and can be found with this article online at http://dx.doi.org/10.1016/j.celrep.2014.06.054.

ACCESSION NUMBERS

The $^{K44A}Dyn_{GTP}$ tube density map has been deposited in the EM Data Bank under accession number EMD-2701. Coordinates for the complete docked tetramer models consisting of the dynamin GG construct, the human dynamin 1 middle/GED stalk, and human dynamin 1 PH domain have been deposited to the Protein Data Bank under the accession numbers 4UUD and 4UUK, representing strand one and strand two of the two-start helical K44A GTP-stabilized polymer.

AUTHOR CONTRIBUTIONS

A.C.S., J.A.H., P.R., and J.S.C. purified proteins and carried out biochemical assays. A.C.S. and J.E.H. collected EM data. S.F. and J.E.H. performed all image processing and computational docking, assisted by J.S.C. and A.C.S. A.C.S., J.S.C., and J.E.H. prepared the manuscript.

ACKNOWLEDGMENTS

This work was supported by the National Institute of Diabetes and Digestive and Kidney Diseases Intramural Research Program. J.S.C. is a Nancy and Peter Meinig Family Investigator in the Life Sciences. We thank Drs. Naiqian Cheng and Dennis Winkler for technical assistance on the FEI Polara; Drs. Jeanne Morin-Leisk, Paula Flicker, and Toshi Kawate for insightful discussions; and Dr. Fred Dyda for his continued support and generosity.

Received: February 14, 2014
Revised: May 8, 2014
Accepted: June 25, 2014
Published: July 31, 2014

REFERENCES

Anggono, V., and Robinson, P.J. (2007). Syndapin I and endophilin I bind overlapping proline-rich regions of dynamin I: role in synaptic vesicle endocytosis. J. Neurochem. *102*, 931–943.

Bashkirov, P.V., Akimov, S.A., Evseev, A.I., Schmid, S.L., Zimmerberg, J., and Frolov, V.A. (2008). GTPase cycle of dynamin is coupled to membrane squeeze and release, leading to spontaneous fission. Cell *135*, 1276–1286.

Bethoney, K.A., King, M.C., Hinshaw, J.E., Ostap, E.M., and Lemmon, M.A. (2009). A possible effector role for the pleckstrin homology (PH) domain of dynamin. Proc. Natl. Acad. Sci. USA *106*, 13359–13364.

Burger, K.N., Demel, R.A., Schmid, S.L., and de Kruijff, B. (2000). Dynamin is membrane-active: lipid insertion is induced by phosphoinositides and phosphatidic acid. Biochemistry *39*, 12485–12493.

Chappie, J.S., and Dyda, F. (2013). Building a fission machine—structural insights into dynamin assembly and activation. J. Cell Sci. *126*, 2773–2784.

Chappie, J.S., Acharya, S., Liu, Y.W., Leonard, M., Pucadyil, T.J., and Schmid, S.L. (2009). An intramolecular signaling element that modulates dynamin function in vitro and in vivo. Mol. Biol. Cell *20*, 3561–3571.

Chappie, J.S., Acharya, S., Leonard, M., Schmid, S.L., and Dyda, F. (2010). G domain dimerization controls dynamin's assembly-stimulated GTPase activity. Nature *465*, 435–440.

Chappie, J.S., Mears, J.A., Fang, S., Leonard, M., Schmid, S.L., Milligan, R.A., Hinshaw, J.E., and Dyda, F. (2011). A pseudoatomic model of the dynamin polymer identifies a hydrolysis-dependent powerstroke. Cell *147*, 209–222.

Chen, Y.J., Zhang, P., Egelman, E.H., and Hinshaw, J.E. (2004). The stalk region of dynamin drives the constriction of dynamin tubes. Nat. Struct. Mol. Biol. *11*, 574–575.

Damke, H., Baba, T., Warnock, D.E., and Schmid, S.L. (1994). Induction of mutant dynamin specifically blocks endocytic coated vesicle formation. J. Cell Biol. *127*, 915–934.

Danino, D., Moon, K.H., and Hinshaw, J.E. (2004). Rapid constriction of lipid bilayers by the mechanochemical enzyme dynamin. J. Struct. Biol. *147*, 259–267.

Egelman, E.H. (2007). The iterative helical real space reconstruction method: surmounting the problems posed by real polymers. J. Struct. Biol. *157*, 83–94.

Faelber, K., Posor, Y., Gao, S., Held, M., Roske, Y., Schulze, D., Haucke, V., Noé, F., and Daumke, O. (2011). Crystal structure of nucleotide-free dynamin. Nature *477*, 556–560.

Ferguson, S.M., and De Camilli, P. (2012). Dynamin, a membrane-remodelling GTPase. Nat. Rev. Mol. Cell Biol. *13*, 75–88.

Ferguson, K.M., Lemmon, M.A., Schlessinger, J., and Sigler, P.B. (1994). Crystal structure at 2.2 A resolution of the pleckstrin homology domain from human dynamin. Cell *79*, 199–209.

Ford, M.G., Jenni, S., and Nunnari, J. (2011). The crystal structure of dynamin. Nature *477*, 561–566.

Henderson, R. (2013). Avoiding the pitfalls of single particle cryo-electron microscopy: Einstein from noise. Proc. Natl. Acad. Sci. USA *110*, 18037–18041.

Heymann, J.B., and Belnap, D.M. (2007). Bsoft: image processing and molecular modeling for electron microscopy. J. Struct. Biol. *157*, 3–18.

Heymann, J.A., and Hinshaw, J.E. (2009). Dynamins at a glance. J. Cell Sci. *122*, 3427–3431.

Kozlovsky, Y., and Kozlov, M.M. (2003). Membrane fission: model for intermediate structures. Biophys. J. *85*, 85–96.

Liu, Y.W., Mattila, J.P., and Schmid, S.L. (2013). Dynamin-catalyzed membrane fission requires coordinated GTP hydrolysis. PLoS ONE *8*, e55691.

Mears, J.A., Ray, P., and Hinshaw, J.E. (2007). A corkscrew model for dynamin constriction. Structure *15*, 1190–1202.

Mears, J.A., Lackner, L.L., Fang, S., Ingerman, E., Nunnari, J., and Hinshaw, J.E. (2011). Conformational changes in Dnm1 support a contractile mechanism for mitochondrial fission. Nat. Struct. Mol. Biol. *18*, 20–26.

Mehrotra, N., Nichols, J., and Ramachandran, R. (2014). Alternate pleckstrin homology domain orientations regulate dynamin-catalyzed membrane fission. Mol. Biol. Cell *25*, 879–890.

Mim, C., Cui, H., Gawronski-Salerno, J.A., Frost, A., Lyman, E., Voth, G.A., and Unger, V.M. (2012). Structural basis of membrane bending by the N-BAR protein endophilin. Cell *149*, 137–145.

Morlot, S., Galli, V., Klein, M., Chiaruttini, N., Manzi, J., Humbert, F., Dinis, L., Lenz, M., Cappello, G., and Roux, A. (2012). Membrane shape at the edge of the dynamin helix sets location and duration of the fission reaction. Cell *151*, 619–629.

Pucadyil, T.J., and Schmid, S.L. (2008). Real-time visualization of dynamin-catalyzed membrane fission and vesicle release. Cell *135*, 1263–1275.

Ramachandran, R., and Schmid, S.L. (2008). Real-time detection reveals that effectors couple dynamin's GTP-dependent conformational changes to the membrane. EMBO J. *27*, 27–37.

Ramachandran, R., Pucadyil, T.J., Liu, Y.W., Acharya, S., Leonard, M., Lukiyanchuk, V., and Schmid, S.L. (2009). Membrane insertion of the pleckstrin homology domain variable loop 1 is critical for dynamin-catalyzed vesicle scission. Mol. Biol. Cell *20*, 4630–4639.

Roux, A., Uyhazi, K., Frost, A., and De Camilli, P. (2006). GTP-dependent twisting of dynamin implicates constriction and tension in membrane fission. Nature *441*, 528–531.

Roux, A., Koster, G., Lenz, M., Sorre, B., Manneville, J.B., Nassoy, P., and Bassereau, P. (2010). Membrane curvature controls dynamin polymerization. Proc. Natl. Acad. Sci. USA *107*, 4141–4146.

Schmid, S.L., and Frolov, V.A. (2011). Dynamin: functional design of a membrane fission catalyst. Annu. Rev. Cell Dev. Biol. *27*, 79–105.

Shnyrova, A.V., Bashkirov, P.V., Akimov, S.A., Pucadyil, T.J., Zimmerberg, J., Schmid, S.L., and Frolov, V.A. (2013). Geometric catalysis of membrane fission driven by flexible dynamin rings. Science *339*, 1433–1436.

Sundborger, A., Soderblom, C., Vorontsova, O., Evergren, E., Hinshaw, J.E., and Shupliakov, O. (2011). An endophilin-dynamin complex promotes budding of clathrin-coated vesicles during synaptic vesicle recycling. J. Cell Sci. *124*, 133–143.

Sweitzer, S.M., and Hinshaw, J.E. (1998). Dynamin undergoes a GTP-dependent conformational change causing vesiculation. Cell *93*, 1021–1029.

Tan, R.K., Devkota, B., and Harvey, S.C. (2008). YUP.SCX: coaxing atomic models into medium resolution electron density maps. J. Struct. Biol. *163*, 163–174.

van der Bliek, A.M., and Payne, G.S. (2010). Dynamin subunit interactions revealed. Dev. Cell *18*, 687–688.

Warnock, D.E., Hinshaw, J.E., and Schmid, S.L. (1996). Dynamin self-assembly stimulates its GTPase activity. J. Biol. Chem. *271*, 22310–22314.

Zhang, P., and Hinshaw, J.E. (2001). Three-dimensional reconstruction of dynamin in the constricted state. Nat. Cell Biol. *3*, 922–926.